7 Longitudinal Optics Measurement and Correction

Longitudinal focusing for a bunched beam is provided by both the change in path length with particle energy and by the time-dependent accelerating voltage. Usually one employs a smooth approximation, i.e., one ignores the discrete locations of the rf cavities, in describing the particle motion. The longitudinal motion can then be modelled by second order differential equations. For small oscillation amplitudes these equations simplify to those of harmonic oscillators.

The longitudinal optics and dynamics are closely linked to the transverse plane, so that 'cross-diagnostics' are possible. For example, an energy oscillation of the beam will result in a transverse oscillation at all places with nonzero dispersion; the signals recorded by a transverse pick-up therefore provide valuable information about the longitudinal dynamics. In analogy to the transverse motion (see Sect. 1.4), the oscillation frequency of the longitudinal or *synchrotron* motion is characterized by the number of oscillations per turn, which, in the longitudinal plane, is called the *synchrotron* tune.

In contrast to the transverse motion, there is an inherent strong nonlinearity which arises from the sinusoidal shape of the accelerating voltage. As a consequence the synchrotron tune decreases with oscillation amplitude and is zero at the separatrix. The separatrix describes the outer boundary of the *rf bucket* in phase space, beyond which particles are no longer contained longitudinally. In electron storage rings, particles outside the rf bucket are quickly lost, since they emit synchrotron radiation and lose energy. In proton storage rings such particles lose the time structure of the bunched beam forming a dc current. This phenomenon, seen at the Tevatron and HERA, has come to be called 'coasting beam' [1][2].

Observables which have a strong influence on the beam dynamics include the dispersion function, the momentum compaction factor, and the chromaticity. The values of the dispersion function together with the local bending radius determine the change in path length with beam energy, i.e., the *momentum compaction factor*. The change in the betatron tune with the beam energy, the *chromaticity*, may also couple the transverse and longitudinal degrees of freedom.

In this chapter, we discuss various techniques for measuring the synchrotron tune, the dispersion, the momentum compaction factor, and the chromaticity.

M. G. Minty et al., *Measurement and Control of Charged Particle Beams,*
https://doi.org/10.1007/978-3-662-08581-3_7

7.1 Synchronous Phase and Synchrotron Frequency

In a storage ring the equations of motion for small deviations from the ideal case can be expressed in terms of the phase difference of a particle within the bunch from the synchronous phase ϕ_s and the relative momentum error $\delta = \Delta p/p$. The synchrotron phase is defined such that a particle without momentum error launched at this phase, with respect to the accelerating rf wave, will arrive at the same phase on all subsequent turns. In linear approximation, the equations of motion are

$$\frac{\mathrm{d}\phi}{\mathrm{d}t} = \left(\alpha_c - \frac{1}{\gamma^2}\right)\omega_{\mathrm{rf}}\delta\,, \tag{7.1}$$

where ω_{rf} is the angular accelerating frequency, α_c the momentum compaction factor (compare (1.37)), γ the particle energy in units of the rest mass, and

$$\frac{\mathrm{d}\delta}{\mathrm{d}t} \approx \frac{e\dot{V}}{\omega_{\mathrm{rf}}\beta^2 E T_{\mathrm{rev}}}\,, \tag{7.2}$$

where the dot denotes a derivative with respect to time, E is the beam energy, and $\beta = v/c$ is the particle velocity in units of the speed of light. The momentum compaction factor α_c is a property of the magnetic focussing lattice of the accelerator (which is typically in the range of 10^{-4}, for high brightness accelerators and future storage rings, and is about 10^{-2} in existing storage rings). Note that the phase variation $\mathrm{d}\phi/\mathrm{d}t$ vanishes for $\gamma = \gamma_{\mathrm{t}} \equiv 1/\sqrt{\alpha_c}$, which is referred to as the transition energy. At this energy the beam is particularly susceptible to perturbations and instabilities. In addition, particular rf manipulations are required during 'transition crossing', such as a π phase jump of the accelerating rf wave. For these reasons, several accelerator complexes avoid this point of operation, by transferring beam from one ring with a small momentum compaction factor, operating below transition, to a second ring, where the energy of the injected beam is already above transition.

The quantity $\dot{V}$ represents the restoring force supplied by the cavity. Specifically, for a low current particle beam, $\dot{V}$ is the slope of the accelerating rf voltage evaluated at the particle position. For $V_{\mathrm{rf}}(t) = \hat{V}\cos(\omega_{\mathrm{rf}}t + \psi)$, where ψ is the phase with respect to an arbitrary reference point, the slope is given by

$$\dot{V} = -\omega_{\mathrm{rf}}\hat{V}\sin(\omega_{\mathrm{rf}}t + \psi)|_{\omega_{\mathrm{rf}}t+\psi=\phi_b(t)} = -\omega_{\mathrm{rf}}\hat{V}\sin\phi_b(t)\,, \tag{7.3}$$

where $\phi_b(t)$ the phase of a particle with respect to the crest of the cavity voltage $\hat{V}$. In the steady state, the phase of the beam centroid is approximately equal to the synchronous phase, i.e., $\langle\phi_b(t)\rangle = \phi_s$, where the angular brackets indicate an average over the beam distribution. In general, since both the external rf wave and the beam-nduced ('wake fields') are nonlinear, this relation is not exactly fulfilled.

The synchronous phase corresponds to the phase at which the energy gain from the accelerating cavities exactly compensates the energy lost per turn.

The total energy loss is $\sum U = U_0 + U_{\rm hom} + U_{\rm par}$, where U_0 is the energy loss per turn per particle due to synchrotron radiation, $U_{\rm hom}$ is the loss due to higher order modes in the cavities, and $U_{\rm para}$ represents all other losses arising, for example, from the interaction of the beam with components of the vacuum system. Taking as a zero phase reference the crest of the accelerating voltage, we have

$$e\hat{V}\cos\phi_s = \sum U \tag{7.4}$$

or

$$\phi_s = \cos^{-1}\left(\frac{\sum U}{e\hat{V}}\right) . \tag{7.5}$$

With this definition of ϕ_s (note that often the synchronous phase is defined with respect to the zero crossing instead), a synchronous phase of $\phi_s = \pi/2$ corresponds to zero energy loss.

A further word of caution may be in order. Equation (7.2) is based on a smooth approximation, which does not take into account the discrete location of the rf cavities used for restoring the particle energy. A more exact treatment would employ difference equations instead. For large high-energy storage rings, such as LEP, where the synchrotron tune may approach the half integer, the exact calculation can become necessary [3, 4].

The overvoltage factor $q = e\hat{V}/\sum U$ is useful for parametrizing the energy acceptance of an electron storage ring. As shown in reference [5], the low current energy aperture for a sinusoidal accelerating voltage is given by

$$\delta_{\rm max} = \sqrt{\frac{U_0}{\pi(\alpha_c - 1/\gamma^2)hE}F(q)} , \tag{7.6}$$

where $F(q)$ is the aperture function

$$F(q) = 2\left[\sqrt{q^2-1} - \cos^{-1}\left(\frac{1}{q}\right)\right] \tag{7.7}$$

and h the harmonic number. The harmonic number h follows from the accelerator circumference C, the rf frequency $f_{\rm rf}$, and nominal particle velocity v, via

$$h = \frac{f_{\rm rf}C}{v} = \frac{f_{\rm rf}}{f_{\rm rev}} , \tag{7.8}$$

where $f_{\rm rev}$ is the revolution frequency.

Equations (7.1) and (7.2) can be combined to give a second order, uncoupled equation, which for small amplitudes ϕ_b or δ further simplifies to the equation of a harmonic oscillator (see (1.43)). The harmonic solutions to this equation are represented by the small amplitude contours in the phase space $(\phi - \delta)$ plot. For small oscillation amplitudes, the constant energy trajectories are ellipses centered about the synchronous phase and energy. The oscillation frequency is called the synchrotron frequency and, at small amplitudes, is given by

$$f_s = \frac{\omega_s}{2\pi} = \sqrt{\frac{(\alpha_c - 1/\gamma^2) he \hat{V} {f_{\rm rev}}^2 \sin\phi_s}{2\pi\beta^2 E}} \,. \tag{7.9}$$

It is convenient to define the synchrotron tune Q_s by normalizing the measurable synchrotron frequency f_s to the beam revolution frequency $f_{\rm rev}$ as

$$Q_s = \frac{f_s}{f_{\rm rev}} = \sqrt{\frac{(\alpha_c - 1/\gamma^2) he \hat{V} \sin\phi_s}{2\pi\beta^2 E}} \,. \tag{7.10}$$

For small amplitude oscillations a particle or bunch returns to the same place in phase space every $1/Q_s$ turns.

If the beam centroid performs synchrotron oscillations, the arrival time of the particle at a beam position monitor (BPM) is modulated at the synchrotron frequency and synchrotron sidebands will appear around every harmonic of the revolution frequency. Stronger sidebands are observed with BPMs located at places with nonzero dispersion, due to the modulation of the transverse beam position at the synchrotron frequency. An example of measured synchrotron sidebands about a revolution harmonic is shown in Fig. 7.1. Note that a nonzero chromaticity gives rise to additional synchrotron sidebands around the betatron tune (not shown).

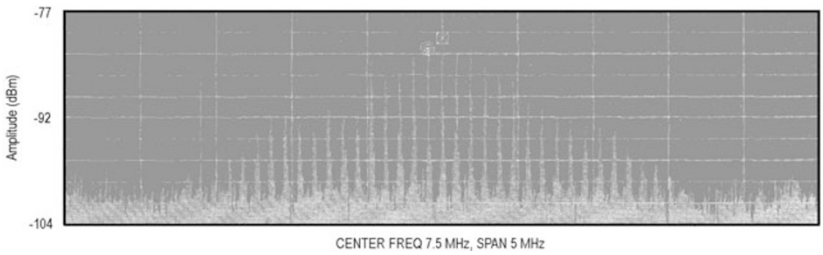

Fig. 7.1. Measurement of multiple synchrotron sidebands at injection in the SLAC electron damping ring. The synchrotron frequency is given by the difference in frequency between the fundamental and the nearest synchrotron sideband

In a manner quite similar to the measurement of the betatron tunes, turn-by-turn BPM measurements may be recorded and Fourier analyzed to detect the modulation of the beam signal due to synchrotron oscillations, e.g., if the selected BPM is in a region of nonzero dispersion. A typical example was shown in Fig. 2.5.

7.2 Dispersion and Dispersion Matching

The horizontal dispersion D_x describes the transverse displacement $x(s)$ of a particle as a function of its relative momentum deviation δ, via

$$x(s) = D_x(s)\delta \,. \tag{7.11}$$

The vertical dispersion is defined analogously. Superimposed on the energy-dependent displacement of (7.11) could be a fast betatron oscillation (cf., (1.6)).

7.2.1 RF Frequency Shift

In most storage rings the dispersion function is inferred from the orbit change induced by a shift in the rf frequency. This measurements makes use of the fact that a frequency shift Δf_{rf} changes the relative momentum deviation of the beam centroid by an amount

$$\delta = -\frac{1}{\alpha_c - \gamma^{-2}} \, \frac{\Delta f_{\mathrm{rf}}}{f_{\mathrm{rf}}} \approx -\frac{1}{\alpha_c} \frac{\Delta f_{\mathrm{rf}}}{f_{\mathrm{rf}}} \, . \tag{7.12}$$

The last approximation, which ignores the change in particle velocity, is usually applicable for electron rings, where $\gamma \gg 1$.

Combining (7.11) and (7.12), we can relate the dispersion to the measured orbit change:

$$D(s) = \left(\gamma^{-2} - \alpha_c\right) \, \frac{\Delta x(s)}{\Delta f_{\mathrm{rf}} / f_{\mathrm{rf}}} \, . \tag{7.13}$$

This 'static' dispersion measurement is quite simple. It requires the capability of being able to smoothly change the ring rf frequency (e.g., to 'unlock' it from the injector rf using an independent voltage controlled oscillator, for example) and a reasonably large energy aperture. By energy aperture we here refer to the range over which f_{rf} can be changed without beam loss. The

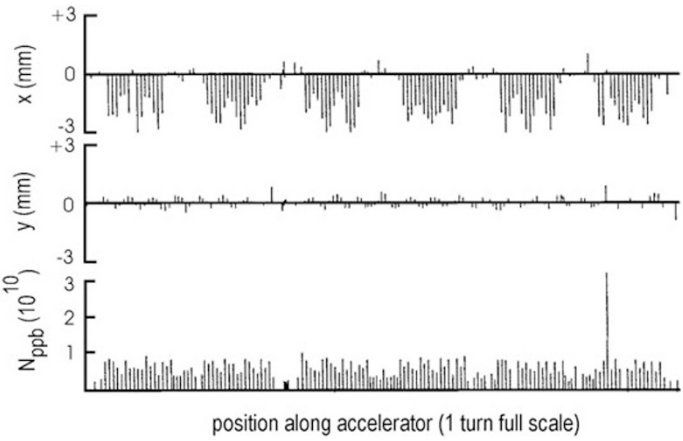

Fig. 7.2. Static dispersion measurement on the PEP-II HER: the orbit change induced by a 2 kHz shift in rf frequency. The nominal rf frequency is 476 MHz, the harmonic number $h = 3492$, and the momentum compaction factor $\alpha_c \approx 0.0024$ (Courtesy U. Wienands, J. Seeman et al., 1998)

residual vertical dispersion is obtained from the vertical orbit shift, in quite the same way as for the horizontal plane.

As an illustration, Fig. 7.2 shows a static dispersion measurement at the PEP-II HER, and Fig. 7.3 a dispersion measurement at the KEK/ATF Damping Ring before and after applying a correction based on exciting steering magnets.

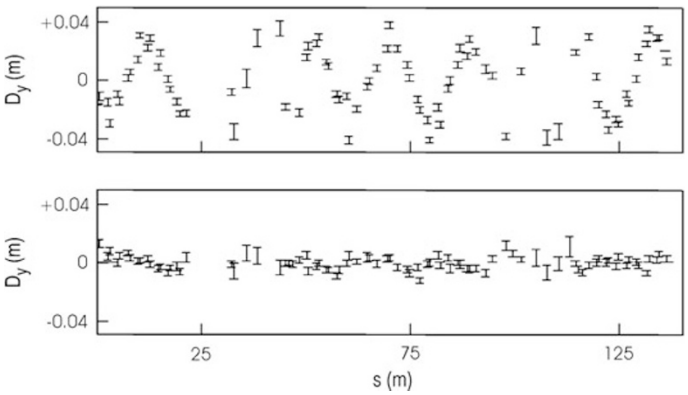

Fig. 7.3. Vertical dispersion measured via a ± 5 kHz rf frequency ramp at the KEK ATF Damping Ring before [*top*] and after correction [*bottom*] [6]; a dispersion of $D_y = 5$ mm corresponded to an orbit change of $\Delta x \approx 15$ μm (Courtesy J. Urakawa, 2000)

7.2.2 RF Modulation

In very large rings, operating at high energy, the above method may not be applicable because of a finite energy aperture and the lack of orbit reproducibility. Therefore, at LEP, a dynamic measurement was occasionally applied [7], where the phase of the rf voltage was harmonically modulated at a frequency close to the synchrotron frequency. Fourier-analysing turn-by-turn BPM data, the frequency component of the induced (resonant) orbit variation at the synchrotron frequency could be inferred, which is proportional to the dispersion at the BPM.

The result of such a dynamic dispersion measurement is displayed in Fig. 7.4. If the dispersion at the cavities is nonzero, the dynamic measurement will give a result different from the static measurement [8]. The reason is that, for nonzero (horizontal) dispersion or nonzero slope of dispersion, an energy change ($\Delta\delta$) due to the rf modulation induces a horizontal betatron motion via $\Delta x_\beta = -D_x\ \Delta\delta$ and $\Delta x'_\beta = -D'_x\ \Delta\delta$. This additional or 'spurious' component of the measured response in amplitude propagates around the ring like a betatron oscillation. In principle, a precise phase measurement from BPM to BPM can be used to correct for this effect.

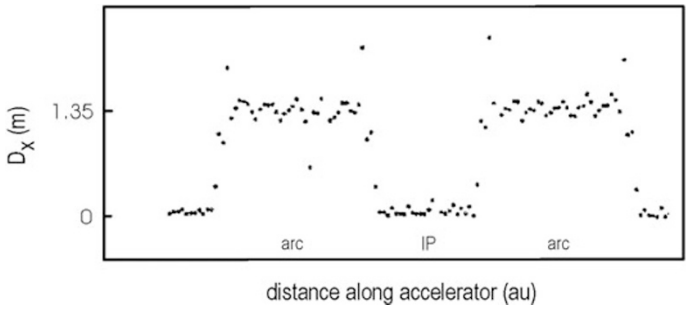

Fig. 7.4. Dynamic dispersion measurement at LEP [7]: the rf voltage was modulated at the synchrotron frequency and the dispersion was deduced by a harmonic analysis of the beam response at each BPM (Courtesy C. Bovet, 1998, G. Morpurgo, 2002)

In the arcs, the maximum value of the spurious dispersion arising from nonzero dispersion at the rf cavities is given by [8]:

$$|\Delta D|_{x,y;\max} = \sqrt{\beta_{x,y}\mathcal{H}_{x,y}} \left| \frac{\sin(2\pi Q_s)\ \sin(\pi Q_{x,y})}{\cos(2\pi Q_s) - \cos(2\pi Q_{x,y})} \right| , \tag{7.14}$$

where $Q_{x,y}$ and Q_s are the betatron and synchrotron tune, respectively, $\mathcal{H}_{x,y} = (D^2_{x,y} + (\alpha_{x,y} D_{x,y} + \beta_{x,y} D'_{x,y})^2)/\beta_{x,y}$ is the dispersion invariant [5] in the straight section, and $\beta_{x,y}$ the beta function in the collider arcs.

7.2.3 RF Amplitude or Phase Jump

Similar dynamic schemes have been tested at the SLC and at the ATF damping rings. In both these rings, a longitudinal oscillation can be induced by a shock excitation: either a sudden step-change to the rf voltage (at the SLC [9]) or a fast phase jump (at the ATF [10]). Like the rf modulation technique, these methods can also give spurious results, if there is residual dispersion at the rf cavities. On the other hand, the dynamic schemes may be used to correct the synchrobetatron coupling, which arises from nonzero dispersion at the rf cavities, by empirically minimizing the spurious dispersion.

7.2.4 Resonant Correction of Residual Dispersion

Since betatron oscillations and residual vertical dispersion propagate around the ring at the same (betatron) frequency, a closed-orbit distortion can resonantly generate a significant dispersion. For this reason, the Fourier spectrum, with respect to the azimuthal position around the ring, of the residual dispersion (normalized to the square root of the local beta function),

$$\tilde{D}_y(k) = \sum_l \frac{D_y(s_l)}{\sqrt{\beta_y(s_l)}} e^{-\mathrm{i}k\frac{\mu(s_l)}{Q_y}} , \tag{7.15}$$

usually contains a large peak at k equal to the integer part of the betatron tune Q_y. In (7.15), the sum is over the ring BPMs, which are located at s_l, and $\mu(s_l)$ denotes the betatron phase at the lth BPM. This 'resonant' dispersion, corresponding to the peak of the Fourier spectrum, can be compensated by special orbit bumps across arcs, as also demonstrated in LEP [11]. Consider an orbit bump of normalized amplitude Y extending over one arc

$$y_{\mathrm{co}} = Y\sqrt{\beta(s)}\sin\left[\mu(s) - \mu(s_i)\right] \ , \tag{7.16}$$

where s_i denotes the start of the arc. The associated dispersion is

$$\begin{aligned} D_y(s) = &- y_{\mathrm{co}} - \frac{Y\sqrt{\beta(s)}}{2\sin(\pi Q_y)} \int_{\mathrm{bump}} \mathrm{d}s' \left[\beta(k_1 - k_2 D_{x,0})\right]_{s'} \cos\left[\pi Q_y \right. \\ &\left. - \left|\mu(s) - \mu(s')\right|\right] \sin\left[\mu(s') - \mu(s_i)\right] \ . \end{aligned} \tag{7.17}$$

Here, k_1 is the quadrupole strength, k_2 the sextupole strength, and $D_{x,0}$ the nominal horizontal dispersion. With a phase advance of 90° per cell, and two families of sextupoles placed near the focusing and defocusing quadrupoles, respectively, from (7.17) the generated dispersion is [11]

$$D_y(s)/\sqrt{\beta(s)} \approx AY \sin\left[\pi Q_y - \mu(s) + \mu(s_i)\right] \ , \tag{7.18}$$

where A denotes the amplification factor for a single arc, and is given by

$$A = \frac{\pi N_{\mathrm{cell}} Q'_{\mathrm{cell}}}{\sin(\pi Q_y)} \, , \tag{7.19}$$

where N_{cell} is the (even) number of regular arc cells covered by the bump, and Q'_{cell} the chromaticity of a single FODO cell.

Bumps across various arcs can be combined in a symmetric or asymmetric manner, so as to cancel and control either the dispersion or the slope of the dispersion at the collision points [11].

7.2.5 Higher-Order Dispersion in a Transport Line or Linac

In a manner similar to that applied in circular accelerators, the dispersion or, more precisely, the R_{16} matrix element in a transport line can be inferred from the measured variation of the beam orbit as a function of the incoming beam energy.

We note that in a transport line the dispersion is not uniquely defined, but depends on the location at which the beam energy is varied. The dispersion or R_{16} (R_{36}) measured in this way does not necessarily correspond to the energy-position correlation within the beam, i.e., for a transport line or linac, in general, we expect that $R_{16} \neq \langle x\delta\rangle/\langle\delta^2\rangle$, where the angular brackets denote an average over the beam. A procedure which directly measures the correlation $\langle x\delta\rangle$ in the beam distribution is described in [12]. It employs

two wire scanners at dispersive locations, separated by an optical $-I$ (minus identity) transformation.

We can extend the concept of dispersion or R_{16} matrix element by including higher-order nonlinear terms[1], of the form:

$$\Delta x(s) = R_{16}(s)\delta + T_{166}(s)\delta^2 + U_{1666}(s)\delta^3 , \tag{7.20}$$

$$\Delta x'(s) = R_{26}(s)\delta + T_{266}(s)\delta^2 + U_{2666}(s)\delta^3 . \tag{7.21}$$

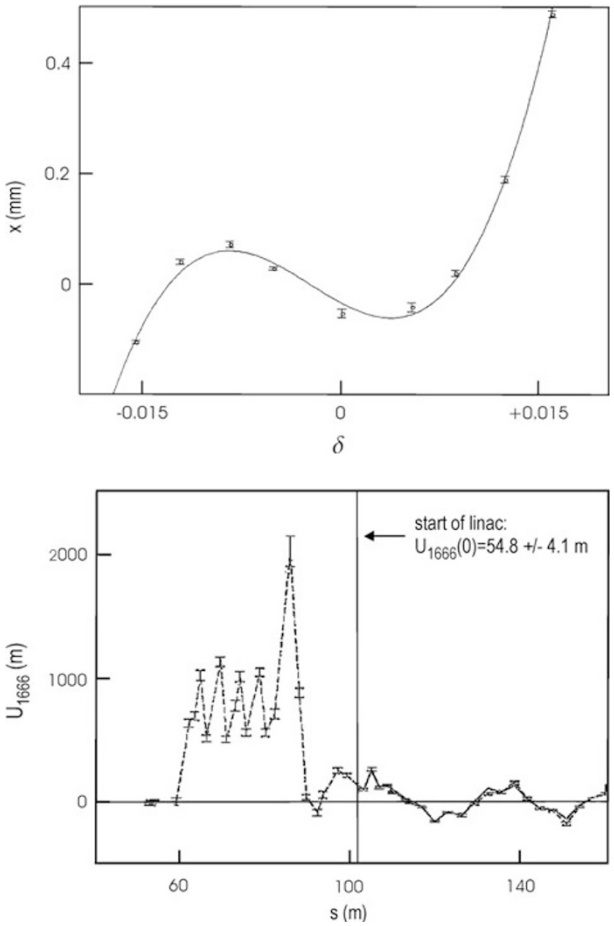

Fig. 7.5. Evidence of 3rd order dispersion in the SLC ring-to-linac transfer line (RTL) [14]: (*top*) Horizontal beam position versus beam energy; (*bottom*) 3rd order dispersion inferred for all BPMs in the RTL and in the early linac. The 3rd order dispersion in the linac is fitted to calculate the magnitude of the U_{1666} and U_{2666} matrix elements (Courtesy P. Emma, 1998)

[1] Here we adopt the notation from TRANSPORT [13].

Sufficiently large energy changes allow a measurement not only of the first-order dispersion matrix element, R_{16}, but also of the 2nd and 3rd order contributions, $T_{166}(s)$ and $U_{1666}(s)$.

Such measurements have been performed at the North ring-to-linac transfer line (NRTL) of the SLC. Under normal operation, the phase of the rf compressor at the entrance to the RTL is set so that the beam center passes at the zero crossing of the rf wave. For a dispersion measurement, the phase is shifted such that the beam center is positioned at the top of the rf crest, and the beam energy is varied by changing the amplitude of the rf voltage.

Figure 7.5 (top) shows the beam position on one of the RTL BPMs as a function of the beam energy. Clearly visible is a nonlinear dependence, which indicates the presence of 3rd order dispersion. The value of the 3rd order dispersion at this BPM can be obtained by fitting a 3rd order polynomial to the measurement. Plotted in the bottom figure is the 3rd order dispersion function obtained from multiple BPMs as a function of position along the RTL and in the early part of the SLAC linac.

The large 3rd order dispersion led to undesired and irrecoverable emittance growth. To correct this, in 1991 two octupole magnets were installed which cancelled the U_{1666} and U_{2666} terms of (7.20) and (7.21). The optimum octupole strength was found by minimizing the linac emittance as a function of the octupole excitation. Such a measurement is shown in Fig. 7.6. The

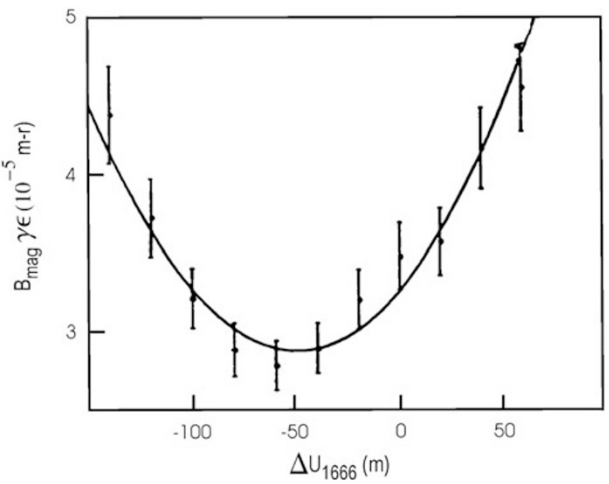

Fig. 7.6. RTL emittance minimization using an octupole for correction of the 3rd order dispersion. Shown on the horizontal axis is change in the octupole strength in units of the generated 3rd order dispersion (ΔU_{1666}). The vertical axis represents the product of B_{mag} (cf. (4.65)) and normalized emittance. The octupole strength for which the emittance is minimum agrees with the magnitude of U_{1666} estimated from the fit in Fig. 7.5 (*bottom*) (Courtesy P. Emma, 1998)

octupole setting for minimum emittance and the corresponding U_{1666} value are in good agreement with the 3rd order dispersion inferred from the BPM readings, which was depicted in Fig. 7.5 (bottom).

7.3 Momentum Compaction Factor

It is sometimes of interest to measure the momentum compaction factor α_c,

$$\alpha_c = \frac{\Delta C/C}{\delta} = \frac{1}{C} \oint \frac{D_x(s)}{\rho(s)} \, \mathrm{d}s \,, \tag{7.22}$$

for example, in storage rings operating near $\alpha_c = 0$ or as a basic check of the accelerator optics. We next present several methods with which to do so.

7.3.1 Synchrotron Tune

If the rf voltage is well calibrated, one can invoke the definition of the synchrotron tune, (7.10), to infer the momentum compaction factor from the measured dependence of the synchrotron tune on $\hat{V}$, taking into account that the synchronous phase angle ϕ_s is also a function of the rf voltage $\hat{V}$. However, often the rf voltage calibration is not very accurate. In addition, if the ring accommodates several rf cavities, these may not be optimally phased with respect to each other, complicating the calculation of the total rf voltage. It is then advantageous to confirm the momentum compaction without having to assume a value for the rf voltage.

Despite the aforementioned difficulties, the synchrotron tune contains information on a variety of parameters, which may be extracted by a judicious choice of measurements and proper fitting strategies. For example, the longitudinal loss factor U may be obtained by measuring the synchrotron tune Q_s as a function of rf voltage $\hat{V}$ for various beam currents, and fitting the result to

$$Q_s^2 = \frac{(\alpha_c - 1/\gamma^2)h}{2\pi} \left(\frac{g^2 e^2 \hat{V}^2}{E^2} + M g^4 \hat{V}^4 - \frac{1}{E^2} U^2 \right)^{1/2} , \tag{7.23}$$

where the $\hat{V}^4$ term is included to account for the discrete locations of the rf cavities. The coefficient M can be computed from the ring optics [3, 15]. An example of a loss-factor measurement using (7.23) is given in Fig. 7.7. From the fit also α_c was determined with a precision better than 10^{-3} (see [15]). In addition, if the beam energy is known at one point, e.g., on a spin resonance, the Q_s vs. $\hat{V}$ curve can be used to calibrate the rf voltage (Fig. 7.8) [15].

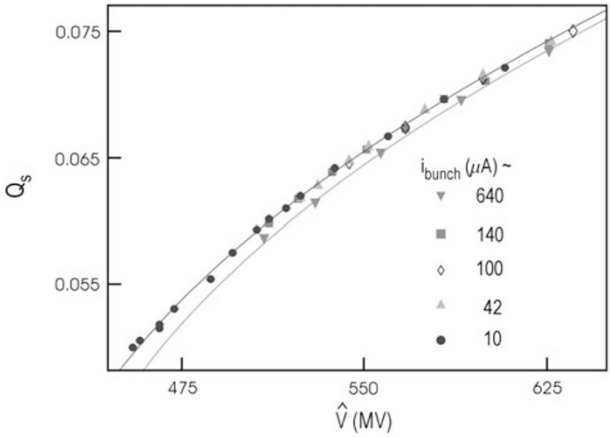

Fig. 7.7. Synchrotron tune Q_s as a function of total rf voltage in LEP; the two curves are fits to the 640 μA and 10 μA data. The difference due to current-dependent parasitic mode losses is clearly visible. Here the nominal beam energy $E_{\rm nom}$ was 60.589 GeV [15] (Courtesy A.-S. Müller, 2000)

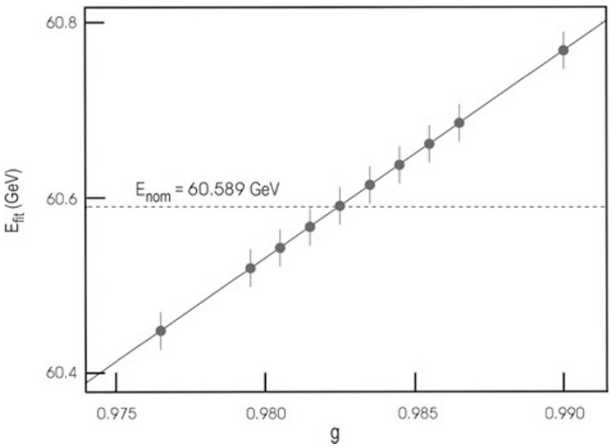

Fig. 7.8. Beam energy fitted from Q_s vs. $\hat{V}$ measurement as a function of rf voltage calibration factor g; the *dotted line* indicates the known energy value, determined independently by resonant depolarization [15] (Courtesy A.-S. Müller, 2000)

7.3.2 Bunch Length

The rms bunch length in an electron or high-energy proton ring can be inferred from the duration of the synchrotron-light pulse using a streak camera. The rms bunch length σ_z is proportional to α_c and to the rms energy spread [5], namely

$$\sigma_z = \frac{c(\alpha_c - 1/\gamma^2)}{2\pi Q_s f_{\rm rev}} \sigma_\delta \,, \tag{7.24}$$

where c is the speed of light and $f_{\rm rev}$ is the revolution frequency. The rms energy spread can either be deduced from the measured decoherence of a transverse oscillation due to nonzero chromaticity and its subsequent recoherence after one synchrotron period (see also (7.36)) [16], or it can be calculated from [5]

$$\sigma_\delta^2 = \frac{C_q \langle G^3 \rangle \gamma^2}{J_\epsilon \langle G^2 \rangle} \,, \tag{7.25}$$

where $C_q = 3.84 \times 10^{-13}$ m, $G = 1/\rho$ the inverse bending radius, $\langle \ldots \rangle$ indicates an average over the ring, γ is the beam energy in units of the particle rest mass, and J_ϵ the longitudinal damping partition number. The value for the latter can be verified by measuring either the horizontal emittance (which is inversely proportional to the horizontal partition number J_x, where $J_x = (3 - J_\epsilon)$ for a planar accelerator) or the longitudinal damping time (cf. (4.74)).

Plotting the measured bunch length as a function of the inverse synchrotron tune immediately gives the value of α_c as the slope [17] from (7.24). Note that the synchrotron frequency $f_s = \omega_s/2\pi$ can be measured very precisely. Figure 7.9 shows a measurement of bunch length vs. synchrotron tune in PEP-II.

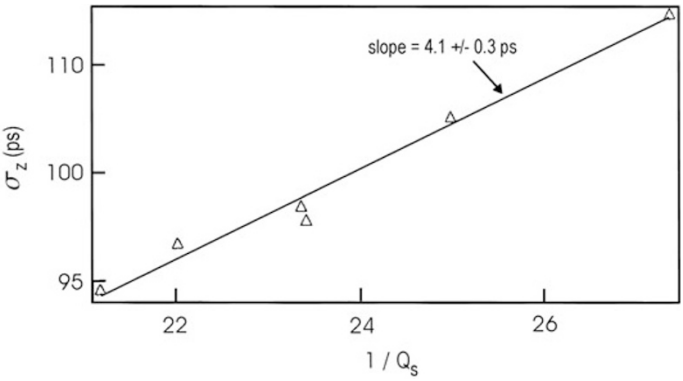

Fig. 7.9. Rms bunch length in the PEP-II HER as a function of the inverse synchrotron tune [18]. The fitted slope determines the momentum compaction factor α_c, if the rms energy spread is known (Courtesy A. Fisher, 1998)

7.3.3 Lifetime

A different approach [17] for determining α_c, applicable for electron rings, is to measure the quantum lifetime [5],

$$\tau_q = \frac{\tau_\delta}{2} \, \frac{e^{\xi_q}}{\xi_q} \,, \tag{7.26}$$

where τ_δ is the longitudinal damping time, and ξ the ratio of the energy aperture $\delta_{\max}$ and the rms relative energy spread σ_δ:

$$\xi_q = \frac{\delta_{\max}^2}{2\sigma_\delta^2} \ . \tag{7.27}$$

A formula for the rms relative energy spread σ_δ was given in (7.25). At low current, the energy aperture, $\delta_{\max}$, if limited by the rf bucket size, is (see also (7.6) and (7.7)) [5]

$$\delta_{\max} \approx \left(\frac{U_0}{\pi(\alpha_c - 1/\gamma^2)hE} F(q) \right)^{1/2} , \tag{7.28}$$

with

$$F(q) = 2\left(\sqrt{q^2 - 1} - \cos^{-1}(1/q) \right) \tag{7.29}$$

and

$$q = \frac{e\hat{V}}{U_0} \ . \tag{7.30}$$

The term $U_0 = C_\gamma E^4 L \langle G^2 \rangle / (2\pi)$ is the energy loss per turn, and $C_\gamma = 8.85 \times 10^{-5}$ m GeV^{-3}.

We may express σ_δ in terms of σ_z using (7.24), and in addition replace the rf voltage $\hat{V}$ in the definition of q by Q_s and α_c, making use of (7.10). We then arrive at an equation for the quantum lifetime τ_q in terms of the measurable quantities Q_s and σ_z, and the unknown parameter α_c. The latter can then be obtained from a fit to data taken at different rf voltages [17].

7.3.4 Path Length vs. Energy

The momentum compaction factor or, in a transport line, the R_{56} matrix element can also be measured directly by changing the beam energy at the entrance to the beamline of interest, and observing the shift in arrival time at the end of that section.

Such measurements were performed to fine-tune the optics in the nominally achromatic arc of the KEKB linac. The time of arrival at the exit of the arc was measured by a streak camera, which converts the time structure of a pulse of synchrotron radiation from a bend, or of optical transition radiation from a target, into a vertical deflection at the CCD camera.

During commissioning of the KEKB linac, the streak camera trigger signal was locked to the linac rf frequency upstream of the arc. The beam energy was varied by adjusting the voltage of the last klystrons prior to the arc. Figure 7.10 shows two measurements of the R_{56}, performed before and after the strengths of a few quadrupoles were adjusted to match the dispersion, as inferred from the energy dependence of the orbit. Figure 7.10 demonstrates that the dispersion match also eliminated the linear component of R_{56}; the

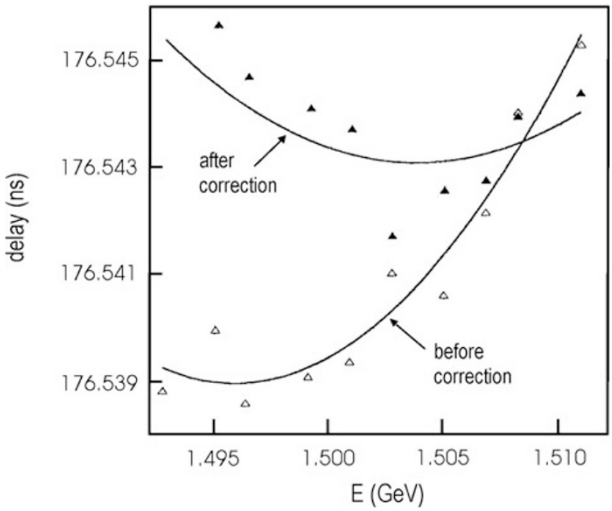

Fig. 7.10. R_{56} measurement for the asynchronous arc of the KEKB linac, before and after dispersion correction. A streak camera was used to measure the arrival time (*vertical axis*) as a function of the beam energy (Courtesy H. Koiso and K. Oide, 1998)

remaining path length dependence on energy is purely quadratic. In the future, it is planned to reduce this quadratic component, as well as the second order dispersion, by adjusting sextupole magnets.

7.3.5 Beam Energy via Resonant Depolarization

In storage rings with polarized beams the beam energy can be determined with a very high precision, using a resonant depolarization technique. The spin tune (see Chap. 10) for an electron is given by

$$\nu_0 = a_e \gamma = \frac{E\ [\mathrm{MeV}]}{440.6486\ [\mathrm{MeV}]}\,, \tag{7.31}$$

where a_e is the electron anomalous magnetic moment. If a radially oscillating field generated by a coil is in resonance with the fractional part of the spin tune, the effect of the field adds up over many turns and the nominally vertical spin vector may precess towards the horizontal plane. The exact value of the resonance frequency determines the beam energy via (7.31).

With this technique, it is possible to precisely measure the energy variation induced by a change in the rf frequency. The slope of this measurement gives the momentum compaction factor:

$$\frac{\Delta p}{p} = \frac{1}{\gamma^{-2} - \alpha_c}\,\frac{\Delta f_{\mathrm{rf}}}{f_{\mathrm{rf}}} \approx -\frac{1}{\alpha_c}\,\frac{\Delta f_{\mathrm{rf}}}{f_{\mathrm{rf}}}\,. \tag{7.32}$$

An application of this technique at LEP is shown in Fig. 7.11.

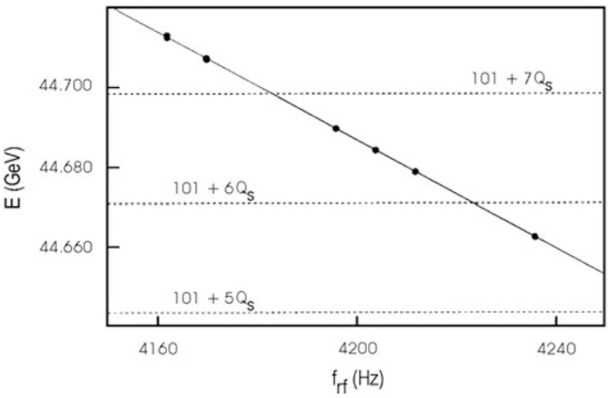

Fig. 7.11. Change of beam energy E as a function of the rf frequency f_{rf} in LEP [19]. Only the last four digits of the rf frequency are shown (the nominal value is $f_{\mathrm{rf}} = 352\ 254\ 170$ Hz). Several strong spin resonances are indicated by the dotted lines. From this measurement the momentum compaction factor was determined to be $(1.86 \pm 0.02) \times 10^{-4}$, which compared well with the calculated value of 1.859×10^{-4} (Courtesy R. Assmann, 1998)

7.3.6 Change in Field Strength for Unbunched Proton Beam

The energy of an unbunched proton beam is constant (neglecting energy losses due to synchrotron radiation for ultrarelativistic beams). If the strength of all magnets (dipoles and quadrupoles) is increased by a factor $\Delta B/B$, the orbit moves inwards and the revolution time is reduced. This change in revolution period Δt can be detected with a Schottky monitor [20]. The momentum compaction factor α_c then simply follows from the relation

$$\frac{\Delta T}{T} = -\left(\alpha_c - 1/\gamma^2\right) \frac{\Delta B}{B}\,, \tag{7.33}$$

where T denotes the revolution period.

7.4 Chromaticity

The dependence of the focusing force on beam energy is generally referred to as chromaticity. In a storage ring this is characterized by the energy dependence of the betatron tunes, which is denoted as $\xi = (\Delta Q/Q)/(\Delta p/p)$ or $Q' = \Delta Q/(\Delta p/p)$. Note that ξ is the normalized chromaticity, related to Q' via $\xi = Q'/Q$.

The natural chromaticity due to the energy dependence of the quadrupole focusing is usually compensated by means of two or more sextupole families at locations with nonzero dispersion. Often a total chromaticity close to zero is desired as this minimizes the tune spread induced by a finite energy spread,

and also the amount of synchrobetatron coupling. The chromaticity should be slightly positive to avoid the head-tail instability. Since a positive chromaticity gives head-tail damping, sometimes Q' is intentionally increased in order to counteract beam instabilities.

7.4.1 RF Frequency Shift

The total chromaticity can easily be determined by measuring the tune shift as a function of the rf frequency f_{rf} using

$$Q'_{x,y} = \frac{\Delta Q_{x,y}}{\Delta p/p} = -\left(\alpha_c - \frac{1}{\gamma^2}\right) \frac{\Delta Q_{x,y}}{\Delta f_{\mathrm{rf}}/f_{\mathrm{rf}}} \,, \tag{7.34}$$

where α_c is the momentum compaction factor. As an example, Fig. 7.12 shows a chromaticity measurement performed at LEP.

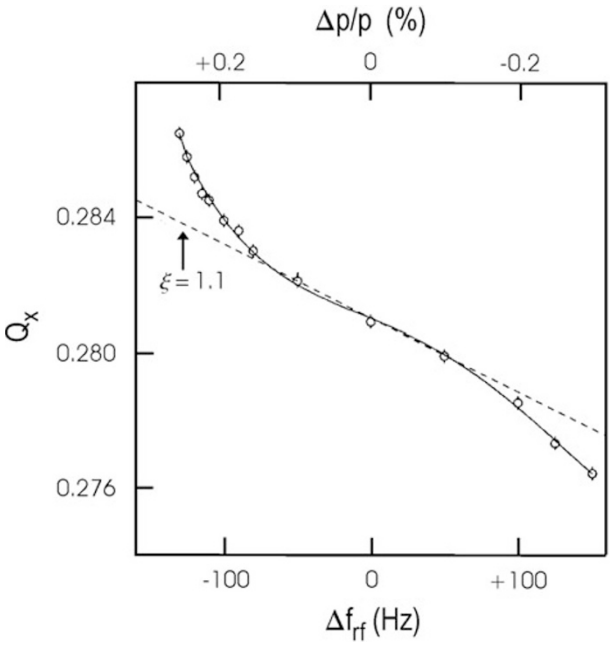

Fig. 7.12. Horizontal tune as a function of the change in rf frequency measured at LEP [21]. The *dashed line* shows the linear chromaticity as determined by the measurements at $\Delta f_{\mathrm{rf}} = \pm 50$ kHz (Courtesy H. Burkhardt, 1998)

7.4.2 Head-Tail Phase Shift

Deflecting the beam transversely and measuring the oscillation of the bunch head and bunch tail separately over a few hundred successive turns also allows the determination of the chromaticity. The underlying relation is [22]

$$\xi_{x,y} = \frac{(\alpha_c - 1/\gamma^2)\Delta\phi(n)}{Q_{x,y}\omega_{\mathrm{rf}}\ \Delta\tau[\cos(2\pi n Q_s) - 1]}\ , \tag{7.35}$$

where $Q_{x,y}$ is the betatron tune, ω_{rf} the angular revolution frequency, $\Delta\tau$ the sample time delay between head and tail signal, and $\Delta\phi(n)$ the phase difference at turn n. After every full synchrotron period, $n = n_s$, the head and tail are again in phase and $\Delta\phi(n_s) = 0$.

The phase at each turn is obtained by a sweeping harmonic analysis, i.e., fitting an oscillation to sets of consecutive data points. The phase difference is determined by simply subtracting the phases of head and tail measured using a wide-band pick-up on each turn. Figure 7.13 shows an example measurement from the CERN SPS, where for technical reasons the phase shift between the head and center of the bunch was detected. The advantage of this method is that it is fast. It will be used to correct rapid changes in the chromaticity at the start of acceleration in the LHC, due to persistent currents in the superconducting magnets.

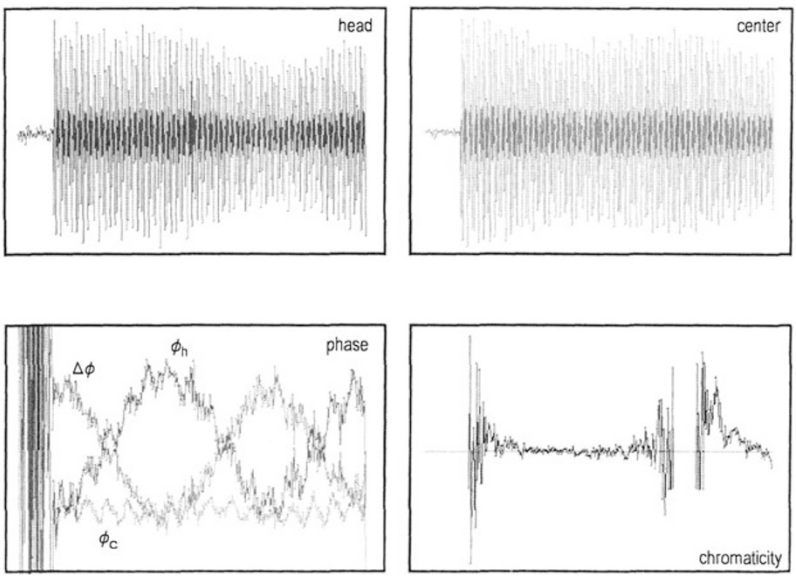

Fig. 7.13. Chromaticity inferred from measurements of the phase shift difference between the head and center of a bunch at the CERN SPS [22]. *Top left*: head oscillation after applying a kick (a.u.); *top right*: center oscillation after the kick (a.u.); *bottom left*: phase of head ϕ_h and center ϕ_c as well as their difference $\Delta\phi$ (with 1.34 radians full scale); *bottom right*: the chromaticity inferred for each turn (with 16.3 units full scale). In all plots the full scale of the horizontal axis is 409 turns (Courtesy R. Jones, 2000)

7.4.3 Alternative Chromaticity Measurements

Other possibilities of measuring the chromaticity include the detection and analysis of synchrobetatron sidebands in the tune spectrum [23] or, as studied at Novosibirsk [24], of the impulse excitation of the beam and the ensuing reversible decoherence due to the chromatic phase.

Due to chromatic beating, the centroid of the 'beam arc' (referring to the beam shape in the transverse phase space) oscillates at the synchrotron frequency. After a vertical impulse excitation, the dipole signal at the betatron frequency is of the form [16]

$$A(t) \propto e^{-\frac{t^2}{2\tau^2}} e^{-\left(\frac{Q'_y}{Q_s}\sigma_\delta\right)^2 (1-\cos\Omega_s t)}, \tag{7.36}$$

where τ is the decoherence time due to the betatron tune shift with amplitude (anharmonicity), and σ_δ is the rms energy spread. For $Q'_y \geq \sigma_\delta Q_s$ separate peaks were seen in the experiment [16]. The width of the peaks is $\tau_E^{-1} = Q'_y \sigma_\delta \omega_0$, which allows measuring either Q'_y or the energy spread σ_δ [16]. We note that in the Novisibirsk experiment, the beam oscillations and decoherence were measured by detecting the synchrotron-radiation photons passing through a limiting half-aperture.

7.4.4 Natural Chromaticity

The natural chromaticity is the chromaticity that derives from the energy dependence of the quadrupole focusing. In other words it is the chromaticity the ring would have without sextupole magnets. Fortunately, to measure the natural chromaticity, it is not necessary to turn off the sextupoles, which might be impossible. Rather the latter can be obtained by detecting the variation of the betatron tune as a function of the main dipole field strength. For an electron beam since the rf frequency is constant, the total path length is constant and the orbit at the sextupoles remains unchanged. The sextupoles therefore do not contribute to a change in tune. (This is a good assumption for FODO lattices, however, it is conceivable that for certain low-emittance lattices the orbit in the sextupoles might change when the dipole field strength is varied. This effect can be estimated with computer codes. One can also monitor the orbit stability at the sextupoles when the dipole field is varied.)

In this case, the absolute beam energy E varies in proportion to the field change: $\Delta E/E = \Delta B/B$. Thus, the natural chromaticity $Q'^{\mathrm{nat}}_{x,y}$ is given by

$$Q'^{\mathrm{nat}}_{x,y} \approx \frac{\Delta Q_{x,y}}{\Delta B/B}\,. \tag{7.37}$$

A typical measurement, from the PEP-II High Energy Ring (HER), is depicted in Fig. 7.14.

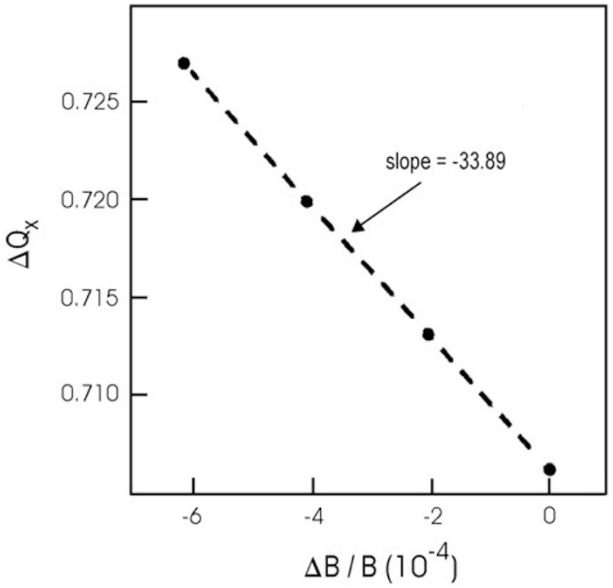

Fig. 7.14. Measurement of the natural chromaticity in the PEP-II HER. Shown is the horizontal tune as a function of relative variation in the main dipole field. The slope of -33.9 is the natural chromaticity inferred from this measurement (Courtesy U. Wienands, J. Seeman et al., 1998)

Similarly, the natural chromaticity can be measured for a proton beam. However, for protons, the rf frequency must be changed in proportion to the dipole field as $\Delta\omega_{,\mathrm{rf}}/\omega_{\mathrm{rf}} = (1/\gamma^2)\Delta B/B$, in order to maintain a constant orbit in the sextupoles.

7.4.5 Local Chromaticity: $\mathrm{d}\beta/\mathrm{d}\delta$

Measuring the beta functions (e.g., with the tune shift method of (2.29)), and using

$$\beta_{x,y} \approx \pm 4\pi \, \frac{\Delta Q_{x,y}}{\Delta k} \, , \tag{7.38}$$

or its more precise equivalent, (2.28), for different values of the rf frequency yields informations on the local chromaticity. This can help to identify the origin of chromatic errors or to find sources of chromatic nonlinearities.

7.4.6 Chromaticity Control in Superconducting Proton Rings

In superconducting proton rings the natural chromaticity is small compared with the chromaticity arising from the persistent-current sextupole components in the dipole magnets. For example, in the HERA superconducting

proton ring the sextupole component in the dipoles contributes a chromaticity that is 5 times larger than the natural chromaticity. At injection energy, a significant part of the persistent current decays in time, causing a large variation in chromaticity. This is illustrated in Fig. 7.15, which also shows the effect of an automatic correction system used at HERA. The correction is done locally by exciting sextupole correction coils mounted inside all bending magnets. The excitation for these correction magnets is determined from the instantaneous sextupole field measured using rotating coils in two reference magnets, which are connected in series with the main superconducting magnet circuit.

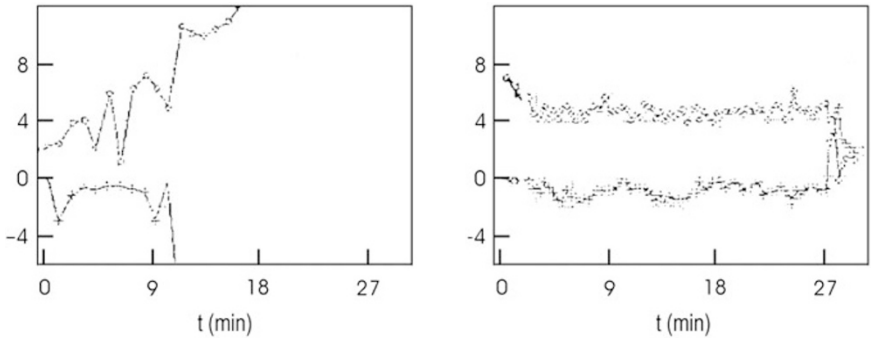

Fig. 7.15. Variation of chromaticity in time, due to persistent-current decay without (*left*) and with (*right*) chromaticity control based on continuous measurements of the sextupole fields in two dipole reference magnets at the HERA proton ring [25]. The horizontal axis is the time in units of 3 minutes per division. The vertical axis refers to the horizontal (*upper trace*) and vertical chromaticity (*lower trace*) in dimensionless units (Courtesy B. Holzer, 1998)

At HERA, the persistent-current sextupole field in the dipole magnets decays during injection at 40 GeV. It is reinduced by the change in dipole field at the start of acceleration, resulting in large variations of the chromaticity. Figure 7.16 shows and example of the change in chromaticity during acceleration from 40 GeV to 70 GeV. The figure compares the actual chromaticity, i.e., the change in tune detected per relative rf frequency change, (7.34), measured without continuous correction; the chromaticity predicted by the reference magnets; and the chromaticity measured with a correction derived from the reference magnets [26].

Another noteworthy feature of the persistent-current sextupole field is that it is not very reproducible from cycle to cycle. At HERA, after each magnet cycle, with the ring magnets set for the injection energy, the chromaticity is first corrected manually by means of a direct measurement (tune shift versus rf frequency). Subsequently, the chromaticity is held constant using the automatic control based on the reference magnets.

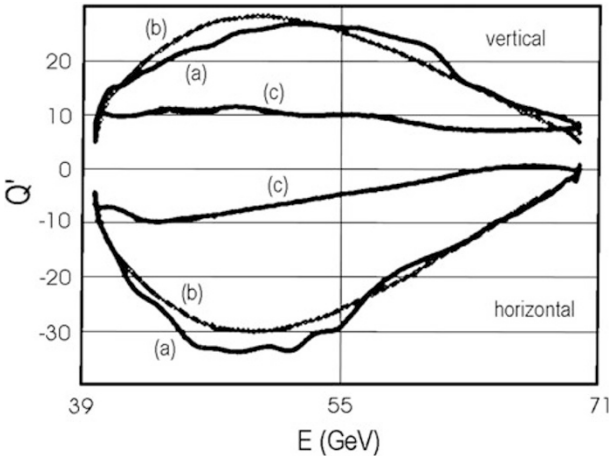

Fig. 7.16. Variation of the chromaticity in the HERA proton ring during acceleration from 40 GeV to 70 GeV [26]: (*a*) measured chromaticity without correction; (*b*) change in chromaticity expected from the reference-magnet measurements; (*c*) measured chromaticity with correction (Courtesy O. Meincke, 1998)

7.4.7 Application: Measuring the Central Frequency

Measuring the chromaticity for different sextupole strengths determines the 'central frequency'. This is the rf frequency for which the orbit on average passes through the center of all sextupoles [27, 28]. An example of such a measurement is shown in Fig. 7.17. Usually adjacent sextupoles and quadrupoles are well aligned with respect to each other, so that one can ex-

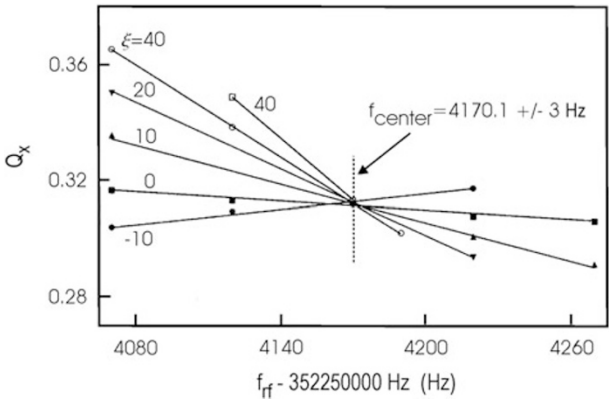

Fig. 7.17. LEP chromaticity measurements for different sextupole excitation patterns with net chromaticities in the range $Q' = -10$ to $+40$ [21]. The intersection of the different lines determines the central frequency, where the orbit is on average centered in the sextupoles (Courtesy H. Burkhardt, 1998)

pect that at the central frequency the beam also passes (on average) through the center of the quadrupoles.

More specifically, four different center frequencies can be measured by changing the strength of the horizontal or vertical sextupole families and by measuring the resulting change in the horizontal or vertical tune, respectively. In most cases, the four central frequencies so obtained are found to be the same, supporting the hypothesis that the magnets are usually well aligned on short length scales.

One can then monitor changes of the beam energy, using the relation

$$\frac{\Delta p}{p} = \left(\frac{1}{\gamma^{-2} - \alpha_c}\right) \frac{\Delta f_{\mathrm{rf}}}{f_{\mathrm{rf}}} \,. \tag{7.39}$$

This energy-monitoring technique was applied at BEPC [29] and LEP [30].

Exercises

7.1 Review of Fourier Transformations and an Application

a) Calculate the Fourier spectrum of the current signal for two bunches of equal charge and asymmetric spacing in a storage ring. Assume that the particle distribution of each bunch can be represented as a δ-function, and that the bunches have equal synchrotron oscillation amplitudes. That is, in the time domain, take the current distribution to be

$$\begin{aligned} i(t) = Q \sum_{n=-\infty}^{\infty} & \delta\left(t - nT - \tau_a \cos(\omega_s n T)\right) \\ & + \delta\left(t - nT - \frac{T}{2} - \Delta t - \tau_a \cos(\omega_s n T + \phi)\right) \,, \end{aligned} \tag{7.40}$$

where Q is the individual bunch charge, T is the revolution period, τ_a is the synchrotron oscillation amplitude, ω_s is the angular synchrotron frequency, Δt is the relative timing offset between the bunches, and ϕ is the relative phase between the two bunches.

Some useful properties of Fourier transformations are:

The Poisson sum rule

$$\frac{1}{2\pi} \sum_{n=-\infty}^{\infty} e^{-2\pi i n(\omega/\omega_r)} = \omega_r \sum_{n=-\infty}^{\infty} \delta(\omega - n\omega_r) \,, \tag{7.41}$$

A Property of Delta-functions

$$\int_{-\infty}^{\infty} f(t)\delta(t-x)\,\mathrm{d}t = f(x) \,, \text{ and} \tag{7.42}$$

The Bessel function sum rule

$$e^{\mathrm{i}z\cos\alpha} = \sum_{k=-\infty}^{\infty} i^k J_k(z) e^{\mathrm{i}k\alpha} \,. \tag{7.43}$$

b) Considering dipole mode oscillations only, sketch the frequency spectrum assuming $\Delta t = 0$ for "0-mode" oscillations (bunches oscillate in phase, that is $\phi = 0$) and for "π-mode" oscillations (for which the bunches oscillate out of phase; i.e., $\phi = \pi$). Show that these two normal modes of oscillation can be distinguished from one another by measuring the frequency spectrum.

c) (Optional) Suppose you wanted to build a passive cavity to damp the π-mode oscillations. (At high beam currents the 0-mode oscillations are Robinson damped.) What would be suitable choices[2] of resonant frequency for the passive cavity assuming (i) and equal bunch spacing ($\Delta t = 0$) or (ii) an unequal bunch spacing. Comment on how the optimum frequency depends on the bunch spacing.

7.2 Adjusting the Incoming Beam Energy

An off-energy beam will have orbit contributions $\Delta x = D_x \delta$ similar to that shown in Fig. 7.2. For a proton beam, the dispersive offset will change on successive turns according to the net bending field and the rf frequency. For electrons the beam will slowly be damped to the on-energy equilibrium orbit due to synchrotron radiation. In either case, describe a procedure using difference orbits at fixed rf frequency for correcting the energy of the incoming beam. Hint: consider a beam injected perfectly into the center of an rf bucket and determine, at which turn one is maximally sensitive to beam energy deviations.

7.3 Resonant Depolarization

Resonant depolarization at the IUCF cooler ring was initially observed at a driving frequency slightly different from expectation assuming the beam energy. Using well-known kinematic reactions with an internal target, the beam energy was precisely determined. Show that the apparent discrepancy can be explained by a small adjustment to the assumed orbit circumference.

7.4 Approximate Expression for the Momentum Compaction Factor

a) Using the approximate formula for the average dispersion function

$$\langle D_x \rangle \approx \frac{\langle \beta_x \rangle}{Q_x} \,, \tag{7.44}$$

and (7.22), show that a good approximation for the momentum compaction factor is given by $\alpha \approx 1/Q_x^2$. Give a numerical example.

b) Find an analogous expression for the transition energy γ_t using these approximations.

[2] we recognize F. Pederson for pointing out the important consequences of unequal bunch spacing in application at the SLC damping rings

7.5 Achieving Design Parameters in the Presence of Unknowns

Suppose upon initial commissioning of an electron storage ring, the beam energy E in the ring, the ring circumference C, and main dipole field B are known to only about $\pm(1-2)\%$. Describe a strategy for setup that ensures the desired beam energy, a dipole field strength matched to this energy, and that dictates the required rf frequency to center the beam in the quadrupoles. Assume that the energy of the injected beam can be determined with a good resolution. Which additional observables could one use to simplify this problem?

7.6 Chromatic Phase Advance[3]

Maintaining the second order driving terms in Hill's equations for the particle motion, we have

$$\begin{aligned} x'' + kx &= kx\delta - \frac{m}{2}(x^2 - y^2)\,, \\ y'' - ky &= -ky\delta + mxy\,, \end{aligned} \tag{7.45}$$

where m is the sextupole strength in units of m^{-3} introduced in Chap. 1 (behind (1.11)).

a) Assuming horizontal dispersion (D_x) only show that

$$\begin{aligned} {x_\beta}'' + kx_\beta &= (k - mD_x)x_\beta\delta\,, \\ {y_\beta}'' - ky_\beta &= -(k - mD_x)y_\beta\delta\,, \end{aligned} \tag{7.46}$$

where the higher-order, so-called geometric aberrations, have been set to zero.

b) Noting that the perturbation in betatron tune may be expressed as

$$\Delta Q = -\frac{1}{4\pi}\int \beta(s)\Delta k(s)\,\mathrm{d}s\,, \tag{7.47}$$

where $\Delta k(s)$ represents the focussing error in units of m^{-2} and $\beta(s)$ the beta function at the location of the error, show that the chromatic phase shifts $\Delta\phi_{x,y}$ over one revolution period for a relative momentum offset δ are given by

$$\begin{aligned} \Delta\phi_x &= -\frac{\delta}{2}\int_s^{s+C} \beta_x(k - mD_x)\,\mathrm{d}s\,, \\ \Delta\phi_y &= \frac{\delta}{2}\int_s^{s+C} \beta_y(k - mD_x)\,\mathrm{d}s\,, \end{aligned} \tag{7.48}$$

where C is the ring circumference.

[3] from text in [31]

c) Using the definition of tune and chromaticity, show that

$$Q'_x = -\frac{1}{4\pi}\int \beta_x(k - mD_x)\,\mathrm{d}s\ ,$$
$$Q'_y = \frac{1}{4\pi}\int \beta_y(k - mD_x)\,\mathrm{d}s\ . \tag{7.49}$$

The first term on the right-hand side of the last two equations represents the natural chromaticity while the second term shows the additive contributions arising from the sextupoles.

Taking into account the second order expansion of the dispersive trajectories (see (1.6)):

$$\begin{pmatrix} x \\ x' \\ y \\ y' \end{pmatrix} = \delta \begin{pmatrix} D_1 \\ D_2 \\ D_3 \\ D_4 \end{pmatrix}\ . \tag{7.50}$$

the chromatic phase shifts for an arbitrarily coupled lattice may be derived. As shown in [32] the chromatic phase advances are given by

$$\Delta\phi_x = -\frac{\delta}{2}\int_s^{s+C} \left[\beta_x({K_x}^2 + k - \lambda D_1) + 2\alpha_x K_x D_2 - \gamma_x(K_x D_1 + K_y D_3)\right]\,\mathrm{d}s\ ,$$
$$\Delta\phi_y = -\frac{\delta}{2}\int_s^{s+C} \left[\beta_y({K_y}^2 + k - \lambda D_1) + 2\alpha_y K_y D_4 - \gamma_y(K_x D_1 + K_y D_3)\right]\,\mathrm{d}s\ ,$$

where λ is an eigenvalue of the one-turn transfer matrix and $\gamma_{x,y}$ is the usual Twiss parameter defined in the plane (x or y) of interest.